Chemistry–A European Journal
Research Article
doi.org/10.1002/chem.202201557
Chemistry Europe
European Chemical Societies Publishing
www.chemeurj.org

Proteophenes – Amino Acid Functionalized Thiophene-based Fluorescent Ligands for Visualization of Protein Deposits in Tissue Sections with Alzheimer's Disease Pathology

Linnea Björk,[a] Marcus Bäck,[a] Linda Lantz,[a] Bernardino Ghetti,[b] Ruben Vidal,[b] Therése Klingstedt,[a] and K. Peter R. Nilsson*[a]

Abstract: Protein deposits composed of specific proteins or peptides are associated with several neurodegenerative diseases and fluorescent ligands able to detect these pathological hallmarks are vital. Here, we report the synthesis of a class of thiophene-based ligands, denoted proteophenes, with different amino acid side-chain functionalities along the conjugated backbone, which display selectivity towards specific disease-associated protein aggregates in tissue sections with Alzheimer's disease (AD) pathology. The selectivity of the ligands towards AD associated pathological hallmarks, such as aggregates of the amyloid-β (Aβ) peptide or tau filamentous inclusions, was highly dependent on the chemical nature of the amino acid functionality, as well as on the location of the functionality along the pentameric thiophene backbone. Finally, the concept of synthesizing donor-acceptor-donor proteophenes with distinct photophysical properties was shown. Our findings provide the structural and functional basis for the development of new thiophene-based ligands that can be utilized for optical assignment of different aggregated proteinaceous species in tissue sections.

Introduction

Protein aggregates composed of fibrils having an extensive cross β-pleated sheet structure are the common pathological hallmark of numerous neurodegenerative diseases, for example Alzheimer's disease (AD), and several fluorescent molecular scaffolds, such as Congo red and thioflavins, targeting these pathological entities have been developed.[1–11] Lately, thiophene-based ligands, such as luminescent conjugated oligothiophenes (LCOs) and bi-thiophene-vinyl-benzothiazoles (bTVBTs), have been applied for fluorescence imaging of protein deposits, and spectral assignment of distinct protein aggregates can be obtained by individual LCOs or combinations of ligands.[12–28] In tissue sections with AD pathology, the two pathological hallmarks, amyloid-β (Aβ) aggregates and tau deposits, can be distinguished by anionic LCOs with a distinct chemical composition,[12–14,16] or by thiophene-based ligands targeting specific aggregated species.[17,20,27] Furthermore, with a dual staining protocol utilizing a tetrameric LCO and a heptameric LCO, age-dependent differences of Aβ deposits in transgenic mice with AD pathology, as well as Aβ aggregate heterogeneity in different etiological subtypes of AD, can be revealed.[15,18,21,24] Overall, thiophene-based ligands with specific chemical composition and distinct optical properties can be utilized as powerful fluorescent tools for assigning protein aggregates in tissue sections with various modes of detection, such as excitation- and emission spectra, as well as fluorescence lifetime imaging (FLIM).[29]

Earlier studies[30–32] have revealed that anionic LCOs, in a similar fashion as Congo Red,[33] interact with regularly spaced cationic lysine residues situated in well-accessible grooves on the protein aggregates, and that the spacing of the carboxylic groups along the oligothiophene backbone influences the affinity of the LCO towards the protein deposits. Thus, electrostatic interactions between the LCO (carboxylic groups) and the protein aggregate (lysine residues) are highly important for efficient binding of the ligand to protein deposits in general. However, while disease-associated protein aggregates seem to share the cross β-pleated sheet structure, recent studies have suggested a conformational variety of aggregates comprised of the same peptide or protein.[18,34–41] Structure determination with cryo-electron microscopy has revealed a structural difference of aggregated tau species between individual tauopathies,[34–38] and fluorescent ligands and biochemical techniques have shown a polymorphism of Aβ deposits in AD.[18,39–41] Hence, it would be of great interest to generate

[a] L. Björk, Dr. M. Bäck, L. Lantz, Dr. T. Klingstedt, Prof. K. P. R. Nilsson
Department of Physics, Chemistry and Biology
Linköping University
581 83 Linköping (Sweden)
E-mail: peter.r.nilsson@liu.se

[b] Dr. B. Ghetti, Dr. R. Vidal
Department of Pathology and Laboratory Medicine
Indiana University School of Medicine
Indianapolis, 46202 Indiana (USA)

Supporting information for this article is available on the WWW under https://doi.org/10.1002/chem.202201557

fluorescent ligands targeting a specific type of protein deposits instead of protein aggregates in general.

Thiophene-based ligands selectively targeting aggregated Aβ or tau pathology in brain tissue sections have recently been presented, and from a chemical perspective, the aggregate selectivity was afforded by replacing distinct thiophene moieties with other heterocyclic building blocks, verifying that chemical modifications of the ligands have a major impact of their binding to distinct protein deposits.[20,27] Herein, we present the synthesis and characterization of pentameric oligothiophenes, denoted proteophenes, with specific amino acid side-chain functionalization along the thiophene backbone (Figure 1). The proteophenes binding properties towards Aβ and tau aggregates in brain tissue sections with AD pathology were evaluated, and alterations of amino acid functionalities of the ligands were shown to reduce or eliminate their capability for identification of distinct aggregated Aβ or tau pathologies. Overall, these findings might aid in the chemical design of ligands recognizing different disease-associated protein aggregates, as well as increase the toolbox of ligands that can be utilized to study the diversity of protein aggregates.

Results and Discussion

Synthesis and photophysical properties of proteophenes with four homologous amino acid functionalities along the thiophene backbone

To generate pentameric proteophenes with a chemical diversity, we selected a pentameric oligothiophene, **3**, functionalized with methyl- and *tert*-butyl esters in orthogonal positions (Scheme 1). The pentamer was achieved by *tert*-butylation of the α-carboxylic acid side chain of a previously reported thiophene dimer **1**,[42] and by applying bromination with N-bromosuccinimide (NBS) in DMF followed by palladium mediated Suzuki-Miyaura cross-coupling reaction to thiophene diboronic acid, the pentameric thiophene was achieved in affordable yield (Scheme 1). From this pentamer, the Li-salt of four different proteophenes, denoted HS-84-E-E, HS-84-K-K, HS-84-Y-Y and HS-84-V-V (Figure 1) were synthesized by repetitive deprotecting reactions under either alkaline or acidic conditions, depending on the protecting group, and hexafluorophosphate azabenzotriazole tetramethyl uronium (HATU)-mediated amide coupling reactions using the methyl- or *tert*-butyl protected L-amino acids tyrosine (Y), glutamic acid (E), valine (V) or lysine (L) (Scheme 2). These four amino acids were chosen to achieve proteophenes having side functionalities with different characteristics, such as polarity, hydrophobicity, and charge. As all the proteophenes have carboxylic groups in the α-positions and β-positions of the pentameric thiophene backbone, the previously reported anionic pentameric LCO, HS-84 (Figure 2A), was also included as a reference ligand.[42,43]

When diluted in phosphate buffered saline (PBS, 10 mM phosphate, 140 mM NaCl, 2.7 mM KCl, pH 7.4), all novel proteophenes displayed similar absorption- and emission characteristics (Figure 1, Supporting Information Figure S1 and Table S1). HS-84-E-E and HS-84-V-V showed an absorption maximum at 418 nm, whereas HS-84-K-K and HS-84-Y-Y displayed a slightly red-shifted absorption maximum at 423 nm and 431 nm, respectively. A similar trend was also observed in the emission mode since HS-84-K-K and HS-84-Y-Y displayed a red-shifted spectrum compared to HS-84-E-E and HS-84-V-V (Figure 1, Supporting Information Figure S1). The most red-shifted emission maximum, 575 nm, was observed for HS-84-K-K, whereas the other three proteophenes showed emission maxima between 545 nm to 550 nm. Similar photophysical characteristics have been observed for other pentameric LCOs[12,13,43] Overall, the photophysical measurements showed that distinct amino acid side-chain functionalities had a minor impact on the basic photophysical characteristic of the respective ligand in PBS.

Histological staining of AD brain tissue sections with proteophenes having four homologous amino acid functionalities along the thiophene backbone

Earlier studies of oligothiophenes have shown that the chemical composition of the ligand has a major influence on the ligand's ability to detect different protein aggregates in AD.[12–14,16] Therefore, we next wanted to examine if a similar behavior could be observed for the proteophenes. To evaluate if the ligands were interacting with Aβ or tau aggregates, the respective proteophene, as well as the previously reported pentameric LCO, HS-84 (Supporting Information, Figure S2),[42,43] was applied for histological staining of human brain tissue sections (frontal cortex) from three cases with AD pathology. Human tissue sections were used since thiophene-based ligands have shown higher affinity towards protein deposits in AD brain compared to in vitro generated recombinant fibrils.[17] As anionic pentameric LCOs have shown nanomolar affinity

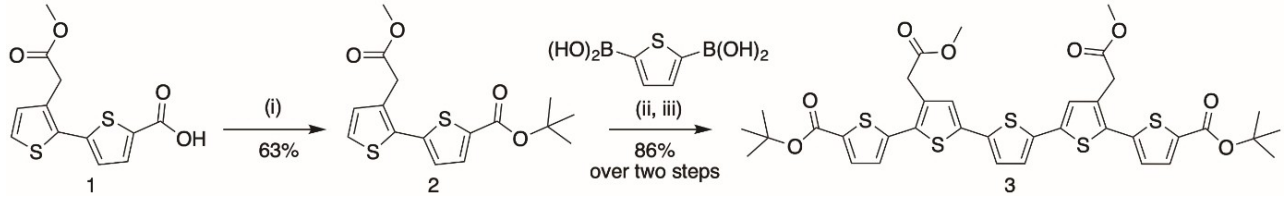

Scheme 1. Synthesis of pentameric oligothiophene functionalized with methyl- and tert-butyl esters in orthogonal positions. Reagents and conditions: (i) 1,4-dioxane, TBTA, $BF_3{\cdot}OEt_2$; (ii) DMF, NBS −15 °C to r.t.; (iii) PEPPSI™-IPr, K_2CO_3, 1,4-dioxane/MeOH (4 : 1), 80 °C.

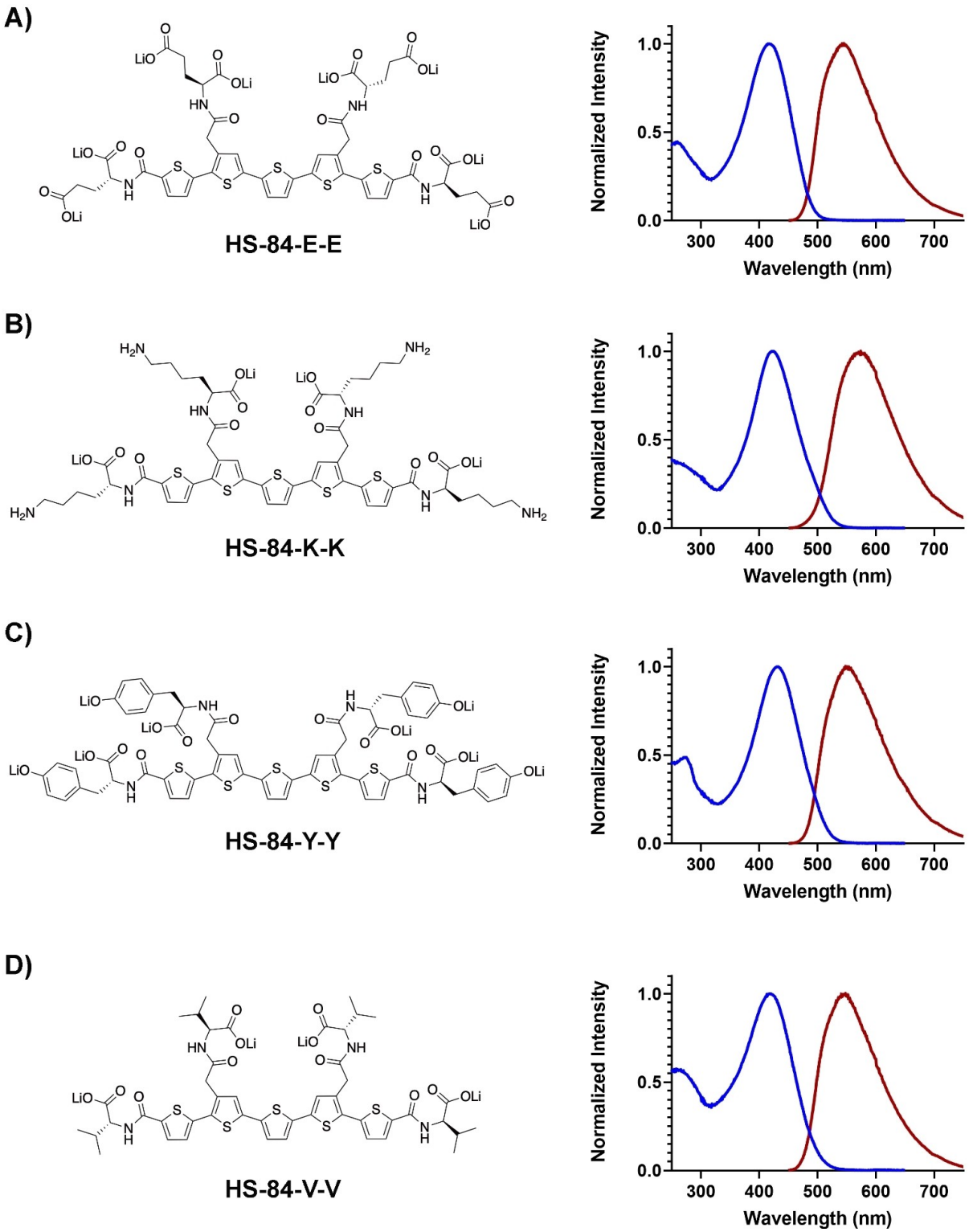

Figure 1. Chemical structure and photophysical properties of the novel proteophenes. Chemical structure (left), absorption- (blue) and emission (red) spectra (right) of the Li-salt of HS-84-E-E (A), HS-84-K-K (B), HS-84-Y-Y (C) and HS-84-V-V (D). The spectra were recorded after diluting each ligand to 30 μM in phosphate buffered saline (PBS, 10 mM phosphate, 140 mM NaCl, 2.7 mM KCl, pH 7.4). For the emission spectra, an excitation wavelength corresponding to the absorption maximum of the respective ligand was used.

towards protein aggregates,[17] 100 nM ligand in PBS was used for staining. With these staining conditions, unspecific binding is avoided and the proteophenes are most likely only binding to the previously reported high-affinity binding site on the

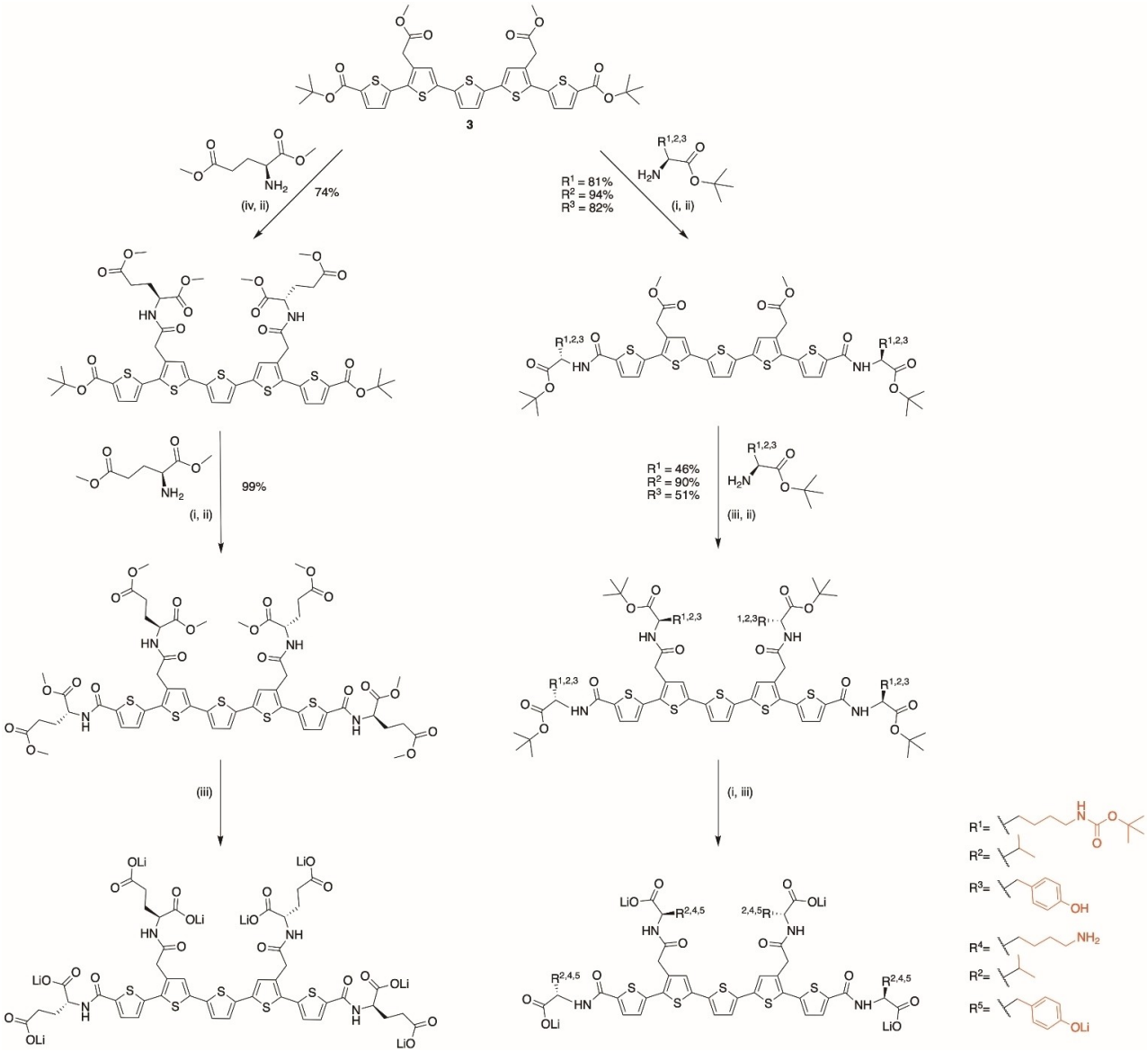

Scheme 2. Synthesis of proteophenes with four homologous amino acid functionalities along the thiophene backbone. Reagents and conditions: (i) DCM/TFA (4:1); (ii) DMF, DIPEA, HATU; (iii) 1,4-Dioxane, LiOH (1 M); (iv) THF, NaOH (1 M).

protein aggregates.[30–32] Previous studies have also shown that when bound to protein aggregates, pentameric anionic LCOs undergo a conformational change that is displayed as a severe red-shift of the absorption- and excitation spectrum.[12,43] Therefore we tested three different lasers, 405 nm, 458 nm or 488 nm, for excitation, and similar to earlier observations,[12,43] the proteophenes displayed the highest emission when using an excitation at 458 nm or 488 nm. When examining the overview of the whole tissue sections with similar imaging conditions (excitation at 488 nm), a variation of staining was observed for the respective ligand (Figure 2). For the sections stained with HS-84, intense fluorescence from several aggregated species was observed throughout the grey matter (Figure 2A) and a similar, but slightly less severe, staining pattern was observed in the section stained with HS-84-E-E (Figure 2B). Furthermore, HS-84-K-K and HS-84-Y-Y labelled sections displayed less staining than HS-84-E-E, whereas the section stained by the fourth proteophene, HS-84-V-V, showed drastically reduced amount of fluorescent aggregated species in the grey matter compared to all other ligands (Figure 2B). Thus, the chemical nature of the amino acid side-chain functionalities of the proteophenes had a major impact on the ligands' ability to detect protein aggregates in AD brain tissue sections. Tissue sections stained with HS-84-Y-Y and HS-84-V-V also displayed a slightly higher background fluorescence in areas containing white matter, suggesting that proteophenes functionalized with hydrophobic amino acids might render more unspecific binding to these regions.

To examine the difference in detection of protein aggregates in AD brain for the respective ligand in more detail, we

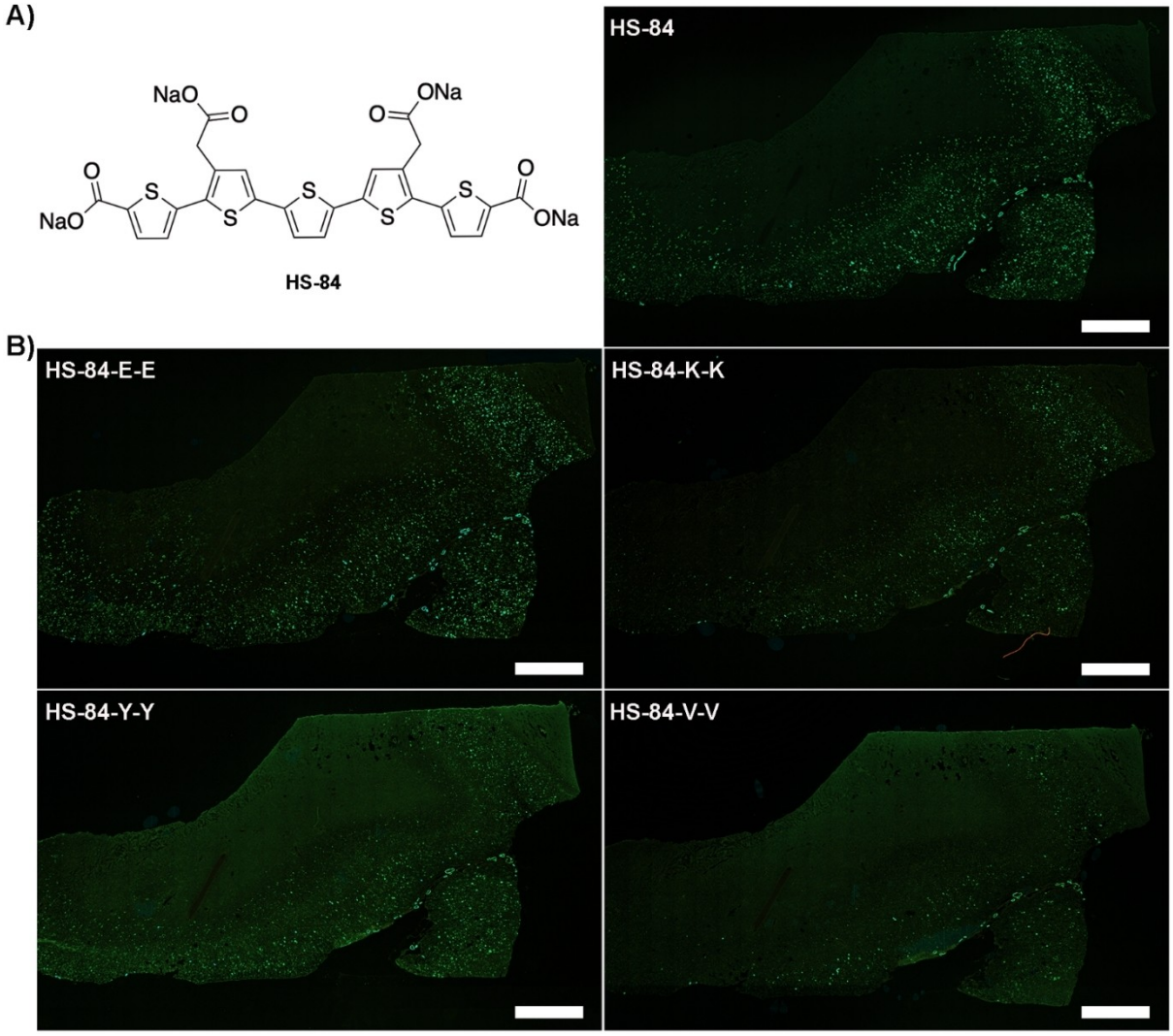

Figure 2. Fluorescent detection of protein aggregates in brain tissue sections with AD pathology stained with different proteophenes. A) Chemical structure (left) of HS-84 and an overview image of the whole tissue section stained with 100 nM HS-84-E-E (right). B) Overview image of the whole tissue section stained with 100 nM HS-84-E-E (top left), HS-84-K-K (top right), HS-84-Y-Y (bottom left) or HS-84-V-V (bottom right). The staining was performed on adjacent sections and the images correspond to 375 tiles taken with a 10× objective. The tile images were recorded in spectral mode using an excitation at 488 nm and collecting the emission between 450 nm to 700 nm. Scale bar represents 2 mm.

next analysed the staining of some characteristic types of immuno-positive aggregated species; Aβ cored plaques, diffuse Aβ plaques, cerebral amyloid angiopathy (CAA) lesions and tau pathology (neuropil threads and neurofibrillary tangles (NFTs)) (Figure 3). The anionic pentameric oligothiophene, HS-84, displayed strong fluorescence from all these aggregated pathologies (Supporting Information, Figure S2). All proteophenes displayed strong fluorescence from CAA lesions and Aβ cored plaques, whereas they showed a discrepancy in staining towards diffuse Aβ plaques (Figure 3). HS-84-E-E and HS-84-Y-Y clearly labelled these aggregated Aβ species, whereas HS-84-K-K displayed weaker staining of this pathology. Notably, with HS-84-V-V, the staining of diffuse Aβ was completely lacking and the absence of staining was also confirmed by co-staining with a previously reported Aβ specific thiophene-based ligand HS-276[27] (Supporting Information, Figure S3). Hence, HS-84-V-V stained strikingly less aggregated Aβ pathology than the other proteophenes, suggesting that valine side-chain functionalities along the pentameric thiophene backbone restricted binding of the ligand to aggregated Aβ species. Likewise, differential staining by the proteophenes could also be observed for aggregated tau pathology (Figure 3). HS-84-Y-Y showed strong and abundant staining of both neuropil threads and NFTs, whereas HS-84-K-K labelled NFTs and some neuropil threads. For HS-84-E-E and HS-84-V-V, only a fraction of the NFTs could be observed, and staining of neuropil threads was lacking for both these ligands. Thus, similar to the observation for Aβ deposits, the chemical nature of the amino acid side chain functionalities influenced the ligands' ability to detect aggregated tau pathology. When bound to the respective aggregated species, all the proteophenes displayed different emission spectra compared to free ligand in PBS (Figures 1, 3 and

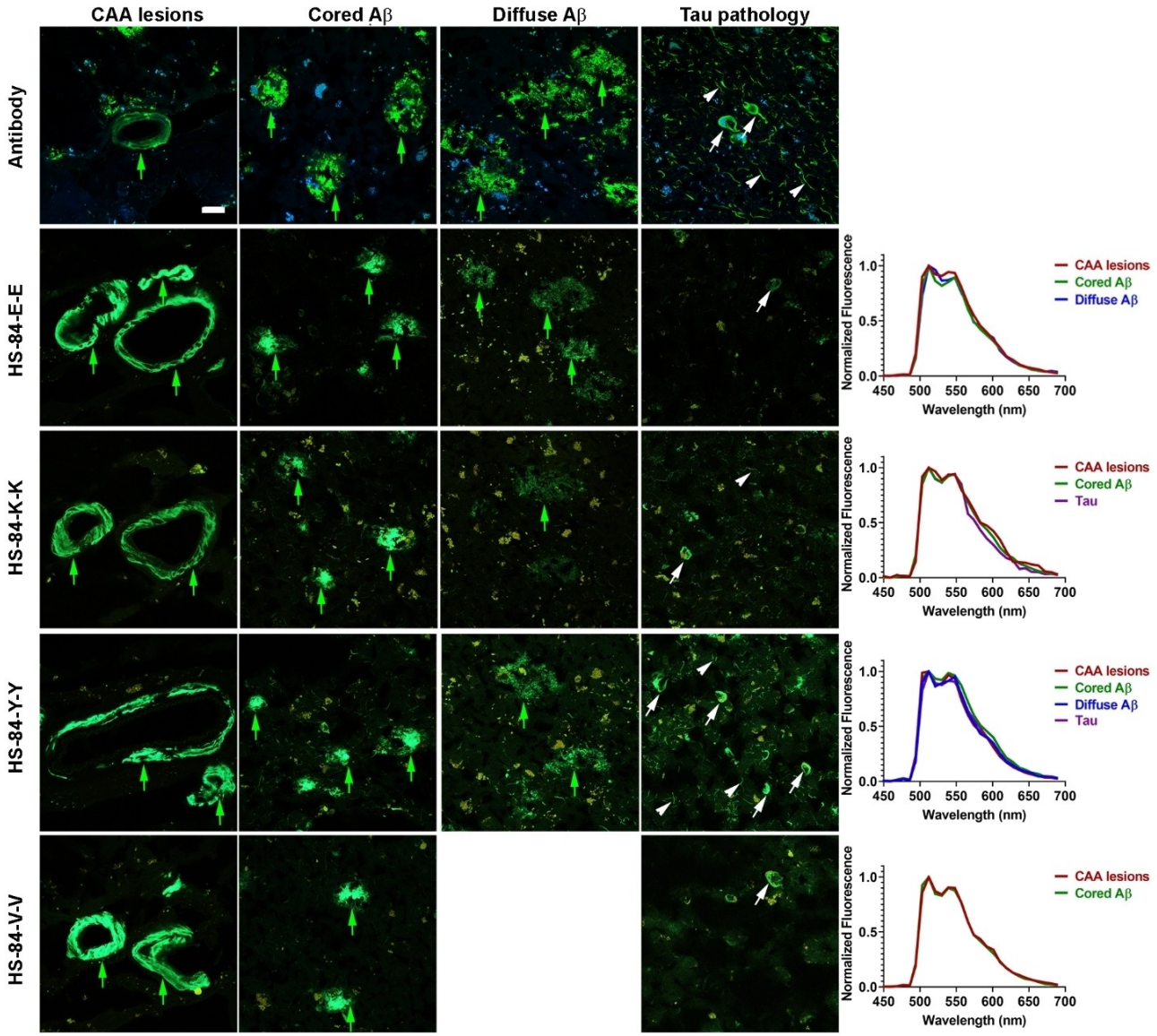

Figure 3. Fluorescent assignment of different Aβ and tau pathologies in AD brain tissue sections stained with different proteophenes. Images and fluorescence spectra from immuno-positive Aβ deposits (green arrows), including cerebral amyloid angiopathy (CAA) lesions, Aβ cored plaques, diffuse Aβ plaques, and tau pathology (white arrows: neurofibrillary tangles (NFTs), white arrowheads: neuropil threads) in tissue sections stained with 100 nM HS-84-E-E, HS-84-K-K, HS-84-Y-Y or HS-84-V-V. Autofluorescence from lipofuscin is seen in blue (top panel) or yellow (ligand staining). The staining was performed on adjacent sections and the images were recorded in spectral mode using an excitation at 488 nm and the emission was collected between 450 nm to 700 nm. Scale bar represents 20 μm.

Supporting Information, Figure S4), verifying that binding to protein aggregates resulted in distinct spectral signatures from the ligands. The characteristic double-peaks in the emission spectra (Figure 3 and Supporting Information Figure S4) have also been observed for other oligothiophenes bound to protein aggregates, and similarly to earlier observations with HS-84, none of the proteophenes displayed a spectral difference bound to Aβ or tau aggregates.[12–14,16,42,43]

Synthesis and photophysical properties of proteophenes with different amino acid functionalities along the thiophene backbone

As the pentameric oligothiophene, **3**, functionalized with methyl- and *tert*-butyl esters in orthogonal positions (Scheme 1), allows synthesis of proteophenes having different amino acid functionalities in the β-positions of the thiophene moieties, or at the terminal α-positions of the pentameric thiophene backbone, we next synthesized four additional proteophenes, denoted HS-84-E-Y, HS-84-Y-E, HS-84-E-V and HS-84-V-E (Figure 4A). Similar as described above, these ligands were synthesized by repetitive deprotecting reactions under either

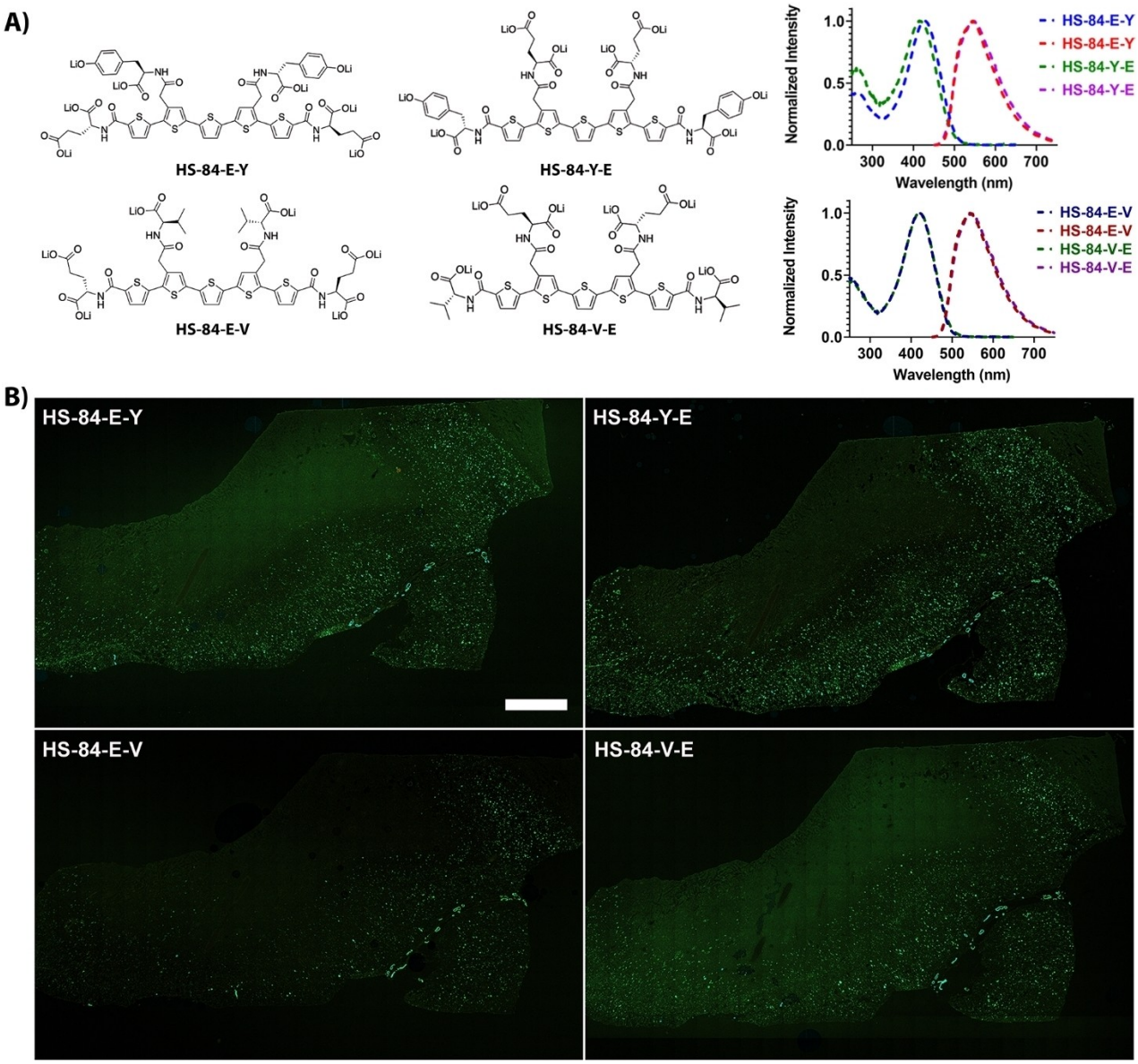

Figure 4. Fluorescent detection of protein aggregates in brain tissue sections with AD pathology stained with proteophenes having different amino acid functionalities along the thiophene backbone. A) Chemical structures, absorption- and emission spectra of the Li-salt of HS-84-E-Y, HS-84-Y-E, HS-84-E-V and HS-84-V-E**. B)** Overview image of the whole tissue section stained with 100 nM HS-84-E-Y (top left), HS-84-Y-E (top right), HS-84-E-V (bottom left) or HS-84-V-E (bottom right). The staining was performed on adjacent sections and the images correspond to 375 tiles taken with a 10× objective. The tile images were recorded in spectral mode using an excitation at 488 nm and the emission was collected between 450 nm to 700 nm. Scale bar represents 2 mm.

alkaline or acidic conditions, depending on the protecting group, and HATU-mediated amide coupling reactions using the methyl- or *tert*-butyl protected L-amino acids tyrosine (Y), glutamic acid (E) and valine (V) (Supporting Information, Scheme S1). These three amino acid side chains were chosen to prove the concept of synthesizing proteophenes with different amino acids in α-positions and β-positions. Positively charged lysine (K) residues were discarded since it might be more problematic to purify zwitter-ionic proteophenes. In PBS, all these ligands showed similar photophysical characteristics, with an absorption maximum around 420 nm and an emission maximum around 545 nm (Figure 4A, Supporting Information Table S1), as the other proteophenes. Thus, analogous to the results obtained for the proteophenes with four homologous amino acid functionalities along the thiophene backbone, variations of the amino acid side chain functionalities had a minor influence on the basic photophysical characteristic of the respective ligand in PBS.

Histological staining of AD brain tissue sections with proteophenes having different amino acid functionalities along the thiophene backbone

Next, we tested HS-84-E-Y, HS-84-Y-E, HS-84-E-V and HS-84-V-E for histological staining. Similar as described earlier, 100 nM of the respective ligand was applied on human brain tissue sections (frontal cortex) from three cases with AD pathology and the tissue sections were analysed with similar imaging conditions (Figure 4B). For HS-84-E-Y, HS-84-Y-E and HS-84-V-E, rather intense staining was observed throughout the grey matter region, whereas HS-84-E-V showed slightly less staining compared to the other ligands (Figure 4B). HS-84-E-Y and HS-84-Y-E displayed intense emission when bound to Aβ cored plaques, diffuse Aβ plaques, CAA lesions, neuropil threads and NFTs, and a similar emission spectrum, with the characteristic double-peaks, was seen from the ligands bound to all these aggregated species (Figure 5). Hence, in contrast to HS-84-E-E (Figure 3), ligands having the glutamates (E) in the α- or β-positions replaced by tyrosines (Y) exhibited strong staining towards both neuropil threads and NFTs, verifying that amino acid functionalities have a major impact on the ligand-protein aggregate interaction. Similarly, HS-84-V-E, the ligand having valines (V) in the α-positions and glutamines (E) in β-positions revealed a strikingly different staining pattern compared to HS-84-V-V (Figures 3 and 5). For HS-84-V-E, all aggregated pathologies of Aβ and tau displayed intense fluorescence, whereas HS-84-V-V only labelled CAA lesions and Aβ cored plaques, as well as a minority of the NFTs. Furthermore, HS-84-V-E also showed a different staining pattern compared to the ligand with only glutamate side chain functionalities, HS-84-E-E, which only labelled a fraction of the NFTs and failed to stain neuropil threads (Figures 3 and 5). Notably, the ligand having glutamates (E) in the α-positions and valines (V) in the β-positions, HS-84-E-V, only stained CAA lesions, Aβ cored plaques and some diffuse Aβ plaques (Figure 5 and Supporting Information, Figure S5), verifying that the distinct positioning of certain amino acid functionalities in the α- or β-positions along the pentameric thiophene backbone influences the ligands' performance in detecting certain aggregated species.

From a chemical perspective, all the proteophenes have carboxylic groups in the α-positions and β-positions, suggesting

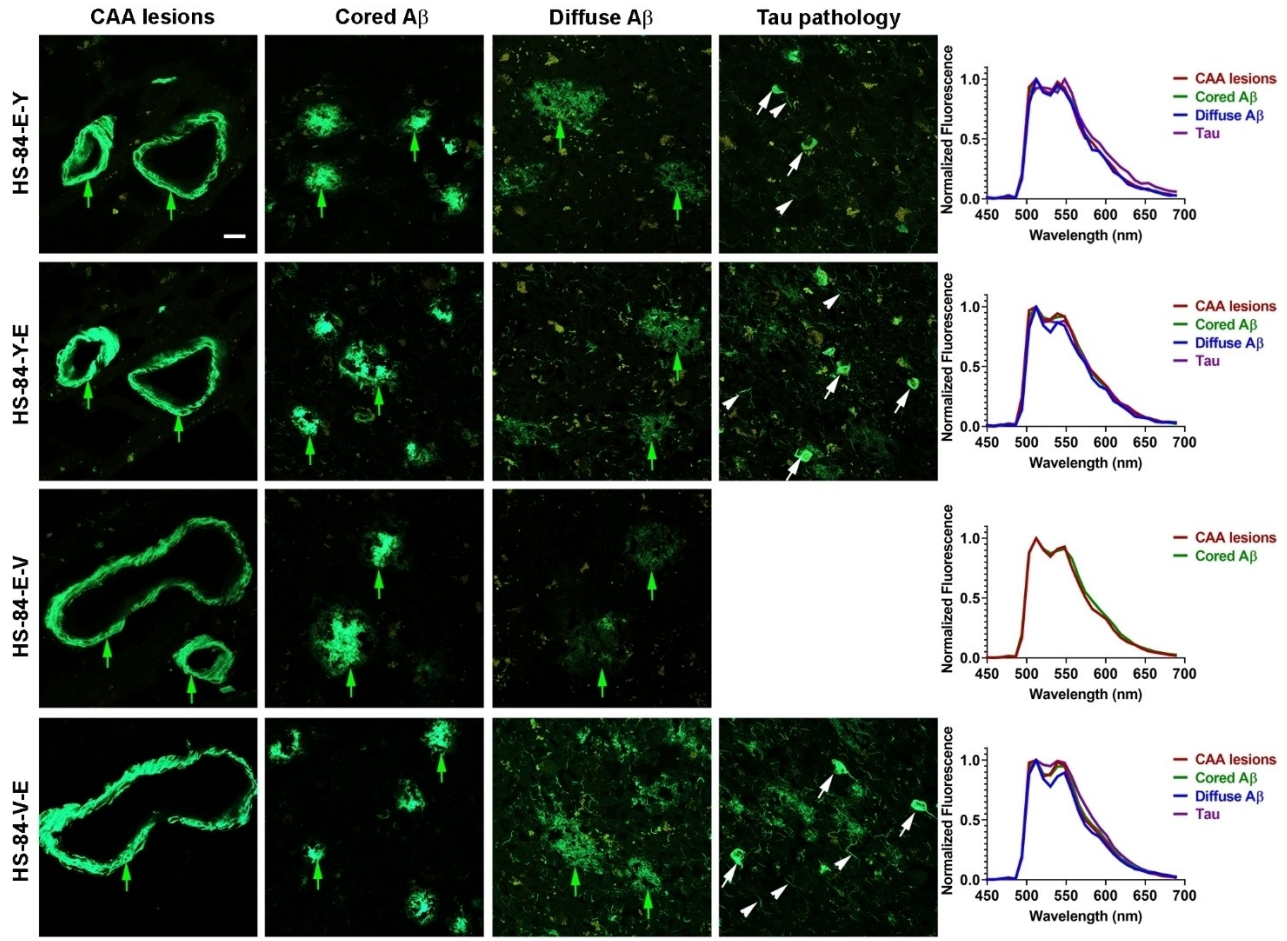

Figure 5. Fluorescent assignment of different Aβ and tau pathologies in AD brain tissue sections stained with different proteophenes. Images and fluorescence spectra from Aβ deposits (green arrows), including cerebral amyloid angiopathy (CAA) lesions, Aβ cored plaques, diffuse Aβ plaques, and tau pathology (white arrows: neurofibrillary tangles (NFTs), white arrowheads: neuropil threads) in tissue sections stained with 100 nM HS-84-E-Y, HS-84-Y-E, HS-84-E-V or HS-84-V-E. Autofluorescence from lipofuscin is seen in yellow. The staining was performed on adjacent sections and the images were recorded in spectral mode using an excitation at 488 nm and the emission was collected between 450 nm to 690 nm. Scale bar represents 20 μm.

that the interaction with the protein aggregates will occur in a similar fashion as reported for anionic LCOs.[30–32] However, the interaction with regularly spaced cationic lysine residues situated in well-accessible grooves on the protein aggregates will most likely be dependent on the chemical nature of the amino acid functionality in the α-positions and β-positions. As shown above, the ligand, HS-84-V-V, having the non-polar isopropyl side chain from valine in both α-positions and β-positions detected less aggregated species than ligands having charged (HS-84-E-E and HS-84-K-K) or uncharged polar side chains (HS-84-Y-Y) from the amino acids in both the α-positions and β-positions (Figures 2 and 3). In addition, proteophenes having uncharged- or non-polar side chains in the α-positions and anionic polar side chains in the β-positions, HS-84-V-E and HS-84-Y-E, displayed intense staining of tau-pathologies, whereas less or no observable staining of aggregated tau species was observed for proteophenes with anionic polar side chains in the α-positions and anionic, uncharged- or non-polar side chains in the β-positions, HS-84-E-E, HS-84-E-Y and HS-84-E-V (Figures 3 and 5). Overall, qualitative analysis of the proteophenes' ability to stain the four characteristic aggregated pathologies, Aβ cored plaques, diffuse Aβ plaques, CAA lesions and tau pathology, in frozen brain tissue from three neuropathologically confirmed cases of AD (Table 1) showed that the chemical nature of the amino acid functionalities at the α- or β- positions along the thiophene backbone had a major influence on the ligands' ability to detect certain aggregated species in AD brain tissue. Hence, properly functionalized proteophenes might offer the possibility to detect specific types of protein aggregates, and the recently obtained cryo-EM structures of a diversity of protein aggregates[34–38,44–46] might aid in assigning distinct binding mode for different ligands. As recently shown,[47] combinatorial experimental/theoretical assessment could be utilized to predict the binding mode, as well as photophysical characteristics, of an AD-tau-specific thiophene-based ligand, b-TVBT4, and similar studies with proteophenes are ongoing in our laboratory to determine their binding modes to different protein aggregates.

Table 1. Proteophene staining of different Aβ and tau pathologies in human AD brain tissue sections.

Proteophene	CAA lesions	Cored Aβ	Diffuse Aβ	Tau pathology
HS-84-E-E	++	++	++	(+)
HS-84-K-K	++	++	(+)	+
HS-84-Y-Y	++	++	++	++
HS-84-V–V	++	++	-	(+)
HS-84-E-Y	++	++	++	++
HS-84-Y-E	++	++	++	++
HS-84-E-V	++	++	(+)	-
HS-84-V-E	++	++	++	++

++ = excellent, + = moderate, (+) = poor, − = no staining.

Synthesis and photophysical properties of a donor-acceptor-donor (D-A-D) based proteophene

As donor-acceptor-donor (D-A-D) thiophene-based ligands have been shown to exhibit different photophysical properties than conventional oligothiophenes,[25,43] we next synthesized a D-A-D based proteophene (Supporting Information, Scheme S2). To achieve a D-A-D type pentameric oligothiophene where the middle thiophene building block was exchanged with a 2,1,3-benzothiadiazole (BTD), thiophene dimer **2** was used as starting material. In this regard, the nitrogen-containing heterocycle, BTD, will be utilized as an effective electron acceptor and the thiophenes as donors. Iridium catalyzed borylation was performed using pinacolborane and 4,4′-di-*tert*-butyl-2,2′-bipyridine (BBBPY) under nitrogen reflux yielding borylated thiophene dimer **4** which was then cross-coupled through a palladium mediated Suzuki-Miyaura reaction to 4,7-dibromo-2,1,3-benzothiadiazole resulting in BTD-pentamer **5** in affordable yield. BTD-pentamer **5** was then functionalized with L-valine using the same HATU-mediated amide coupling procedure as described above, and after deprotection, the D-A-D thiophene based ligand, HS-169-V-V (Figure 6A), was afforded. Diluted in PBS, HS-169-V-V showed different absorption- and emission characteristics compared to the pure thiophene-based proteophenes. The ligand showed three absorbance bands between 230 nm and 600 nm (Figure 6A). The two most red-shifted bands likely arise from the π-π* transition and the charge-transfer transition, respectively.[25,43,48] Upon excitation corresponding to the respective absorption band, HS-169-V-V displayed a similar emission with a maximum around 720 nm for both excitation wavelengths (Figure 6A). Similar absorption- and emission profiles have also been observed for the pentameric D-A-D thiophene based ligand HS-169.[43] Overall, the photo-physical measurements verified that HS-169-V-V displayed distinct photophysical properties due to the incorporation of the central BTD moiety and that the chemical composition had a great impact on the photophysical characteristic of the ligand.

Histological staining of AD brain tissue sections with HS-169-V-V

Previous studies[25,45,48] have shown that D-A-D thiophene-based ligands can be used for hyperspectral- or fluorescence lifetime imaging (FLIM) of protein aggregates in AD brain tissue. To examine if HS-169-V-V can be applied in a similar fashion, we next tested the ligand on brain tissue sections with AD pathology. In the same manner as for the other proteophenes, 100 nM of ligand was applied for histological staining, and when examining the tissue sections, bright emission was only observed from CAA lesions, whereas staining of other aggregated Aβ species and tau pathology was lacking (Figure 6B). Thus, HS-169-V-V detected even less aggregated species than the corresponding pentameric oligothiophene HS-84-V-V, suggesting that the replacement of the central thiophene moiety with a BTD motif influences the binding mode of the ligand. In

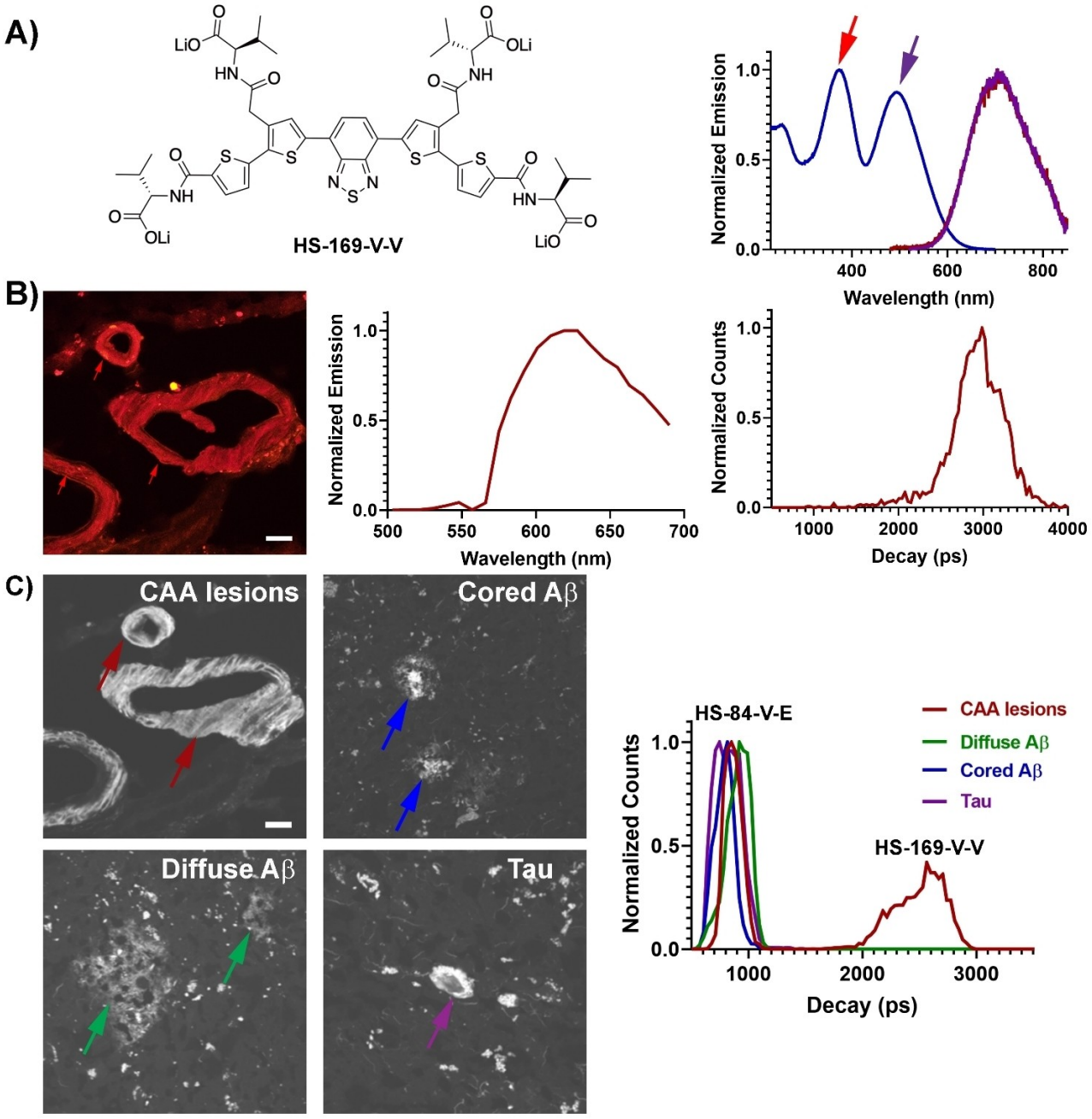

Figure 6. Fluorescent detection of protein aggregates in brain tissue sections with AD pathology stained with a D-A-D based proteophene. A) Chemical structures, absorption- (blue) and emission spectra (red, purple) of the Li-salt of HS-169-V-V. The emission spectra were recorded with excitation wavelengths corresponding to the two absorption maxima, 375 nm (red arrow) or 495 nm (purple arrow). B) Spectral image, fluorescence spectra and fluorescence lifetime distribution of cerebral amyloid angiopathy (CAA) lesions (red arrows) in a tissue section stained with 100 nM HS-169-V-V. The images were recorded in spectral mode using an excitation at 561 nm and the emission was collected between 500 nm to 690 nm Scale bar represents 20 μm. C) Intensity images and fluorescence lifetime distributions from CAA lesions (red arrows), cored Aβ plaques (blue arrows), diffuse Aβ plaques (green arrows) or tau pathology (purple arrow) in a tissue section stained with 100 nM HS-169-V-V and 100 nM HS-84-V-E. The images were recorded using an excitation at 490 nm and the fluorescence lifetime distributions were recorded using excitation at 490/565 nm. Scale bar represents 20 μm.

addition, the length of the accumulated Aβ peptides is different in parenchymal deposits compared to vascular Aβ deposits,[49–51] hence, the preferential binding of HS-169-V-V to CAA lesions might be due to differences in the biochemical composition of the protein aggregates. When bound to CAA lesions, HS-169-V-V showed a blue-shifted emission spectrum with a maximum around 615 nm, compared to the ligand in PBS, as well as a distribution of fluorescence lifetimes between 2000 ps to 4000 ps (Figure 6). Similar decays have also been observed for other D-A-D thiophene-based ligands when bound to protein aggregates.[48]

To examine the lack of binding of HS-169-V-V to Aβ cored plaques, diffuse Aβ plaques and aggregated tau pathology in more detail, we compared the staining result of HS-169-V-V with the previously reported D-A-D thiophene based ligand HS-169 (Supporting Information, Figure S6A).[43] In comparison to HS-169-V-V, HS-169 has carboxylates in the α-positions and the β-positions, but is lacking the non-polar side chain from valine, the isopropyl group, in these positions. When using 100 nM ligand, HS-169 clearly labelled all aggregated Aβ pathologies, as well as neuropil threads and NFTs (Supporting Information, Figure S6B). Thus, similar as shown above for the other proteophenes, adding amino acid side chain functionalities in the α-positions and β-positions influences the ligand's ability to detect different aggregated species.

Since the pure thiophene-based proteophenes and the D-A-D based proteophene ligand exhibit different photophysical properties and differential staining patterns, a dual staining protocol combining HS-169-V-V and HS-84-V-E was applied on brain tissue sections with AD pathology. Similar to the observations above, HS-84-V-E stained all aggregated species, including CAA lesions, cored and diffuse Aβ plaques, as well as tau pathology, and ligand staining could be identified with FLIM (Figure 6C). The ligand displayed intensity weighted mean lifetime distributions between 600 ps and 1000 ps, which is similar to other pentameric oligothiophenes.[29] In contrast, the characteristic longer lifetime distributions, 2000 to 3000 ps, from HS-169-V-V emission could only be observed from CAA, whereas these longer decay times was completely lacking for all the other aggregated species (Figure 6C). Thus, these experiments verified that HS-169-V-V only labelled CAA lesions and signified that a dual staining protocol with a combination of a pure thiophene-based proteophene and a D-A-D based proteophene can be utilized for assignment of distinct aggregated species in tissue sections.

Conclusion

In conclusion, we have developed a new set of amino acid thiophene-based ligands, denoted proteophenes, with different amino acid side-chain functionalities along the conjugated backbone. Depending on the chemical nature of the side-chain functionalities in the β-positions of the thiophene moieties, or at the terminal α-positions of the pentameric thiophene backbone, the ligands selectively targeted different Aβ or tau pathologies in AD brain tissue sections. In addition, a D-A-D based proteophene with alternative photophysics compared to the pure thiophene-based proteophenes was presented, and a dual staining protocol allowing multiplex photophysical detection of distinct protein aggregates in tissue sections with AD pathology was afforded when combining different proteophenes. Our findings provide useful knowledge of how minor chemical changes of the proteophenes influence their binding properties towards different protein aggregates, as well as expand the toolbox of fluorescent ligands that can be utilized for fluorescent assignment of distinct aggregated proteinaceous species. We foresee that proteophenes will aid in studying the pathological relevance of distinct protein deposits in several protein aggregation diseases.

Experimental Section

Full experimental details including additional characterization data and NMR spectra of new compounds, as well as supporting figures and schemes are given in the Supporting Information.

Synthesis of ligands: The synthesis of compound **1**, HS-84, HS-169, b-TVBT2 and HS-276 has been published elsewhere.[20,27,42,43] The detailed synthesis of the proteophenes is described in the Supporting Information (Supporting Information).

Optical characterization of the ligands: Stock solutions of ligands (1.5 mM in de-ionized water) were diluted to 30 μM in in phosphate buffered saline (PBS, 10 mM phosphate, 140 mM NaCl, 2.7 mM KCl, pH 7.4). Excitation- and emission spectra of the ligands were collected using an Infinite M1000 Pro microplate reader (Tecan, Männedorf, Switzerland).

Immunohistochemistry: Frozen brain tissue from three neuropathologically confirmed cases of Alzheimer's disease (AD) was obtained from the Dementia Laboratory at the Department of Pathology and Laboratory Medicine, Indiana University School of Medicine, Indianapolis, USA. The studies carried out at the Indiana University School of Medicine were reviewed and approved by the Indiana University Institutional Review Board and informed consent was obtained from the patient or their next of kin. The experiments performed at Linköping University were reviewed and approved by a national ethical committee (approval number 2020–01197). Frontal cortex AD brain tissue sections (10 μm) were fixed in pre-cooled acetone at −20 °C for 5 min. After drying for 30 min at RT, the sections were incubated in phosphate buffered saline (PBS, 10 mM phosphate, 140 mM NaCl, 2.7 mM KCl, pH 7.4) for 1 min to remove OCT embedding compound, and then in PBS with 5% normal goat serum (blocking buffer) for 30 min to block unspecific binding. The sections were then incubated with 4G8 antibody (Biolegend) directed against Aβ or GT-38 antibody (Abcam) directed against tau for 2 h at RT. Both antibodies were diluted 1 : 1000 in blocking buffer. After washing in PBS for 3 × 5 min, the sections were inbubated for 1 h at RT with goat anti-mouse secondary antibody conjugated with Alexa Fluor 488 diluted 1 : 400 in blocking buffer. The sections were then washed with PBS and mounted using Dako mounting medium for fluorescence (Agilent). The staining result was analyzed using an inverted Zeiss 780 confocal laser scanning microscope (Zeiss).

Ligand staining: Sections of frontal cortex (10 μm) from three AD cases were fixed in 96% EtOH for 10 min at RT, incubated 10 min in 50% EtOH followed by 10 min in dH_2O at RT and then 10 min in PBS. The sections were incubated with 100 nM of the respective ligand in PBS for 30 min at RT. The sections were then washed with PBS three times and mounted with Dako mounting medium for fluorescence (Agilent). The mounting medium was allowed to solidify at least overnight before sealing the cover slips with nail polish. The sections were analysed using an inverted Zeiss LSM 780 laser scanning confocal microscope (Zeiss) using excitation at 488 nm or 561 nm for spectral imaging.

Ligand double staining: Sections of frontal cortex (10 μm) from three AD cases were fixed, rehydrated and incubated in PBS as described above (ligand staining). The sections were then incubated with a combination of ligands, 100 nM HS-169-V-V and 100 nM HS-84-V-E, 200 nm HS-276[4] and 100 nM HS-84-V-V, or 100 nM b-TVBT2[3] and 100 nM HS-84-E-V, for 30 min at RT. The sections were then washed with PBS three times and mounted with

Dako mounting medium for fluorescence (Agilent). The mounting medium was allowed to solidify at least overnight before sealing the cover slips with nail polish. The sections with the different combination of ligands were analysed using an inverted Zeiss LSM 780 laser scanning confocal microscope (Zeiss) with the following settings; HS-169-V-V/HS-84-V-E: excitation at 458 nm or 561 nm for spectral imaging, as well as 490 nm and 565 nm for fluorescence lifetime imaging (FLIM).HS-276/HS-84-V-V: excitation at 405 nm or 458 nm for spectral imaging.b-TVBT2/HS84-E-V: combined excitation at 458 nm and 561 nm for spectral imaging.

Fluorescence lifetime imaging (FLIM): Fluorescence lifetime images were acquired using the same confocal microscope system as described above and the data were recorded by a Becker & Hickl Simple-Tau 152 system (SPC-150 TCSPC FLIM module) with the instrument recording software SPCM version 9.42 in the FIFO image mode using 256 time channels (Becker & Hickl GmbH, Berlin, Germany). For all acquisitions, the pinhole was set to 20.2 μm, and for excitation at 490 nm (HS-84-V-E) or 565 nm (HS-169-V-V), a pulsed tunable In Tune laser with a repetition rate of 40 MHz was used. Data was analyzed in SPCImage version 3.9.4 (Becker & Hickl GmbH, Berlin, Germany). As described previously,[29] decays were fitted to a bi-exponential decay and the associated lifetimes and weights were used to calculate an intensity average lifetime for plots and comparison.

Acknowledgements

Our work is supported by the Swedish Research Council (2016-00748), the Swedish Brain Foundation, the Swedish Alzheimer Foundation, the Torsten Söderberg Foundation and the U.S. National Institutes of Health (U01NS110437).

Conflict of Interest

The authors declare no conflict of interest.

Data Availability Statement

The data that support the findings of this study are available from the corresponding author upon reasonable request.

Keywords: Alzheimer's disease · amyloid-β · fluorescent ligands · protein aggregates · tau

[1] A. T. Petkova, Y. Ishii, J. J. Balbach, O. N. Antzutkin, R. D. Leapman, F. Delaglio, R. Tycko, *Proc. Natl. Acad. Sci. USA* **2002**, *99*, 16742–16747.
[2] A. Ross, M. A. Poirier, *Nat. Med.* **2004**, *10*, S10-S17.
[3] F. Chiti, C. M. Dobson, *Annu. Rev. Biochem.* **2006**, *75*, 333–366.
[4] D. Eisenberg, M. Jucker, *Cell.* **2012**, *148*, 1188–203.
[5] H. Bennhold, *Muench. Med. Wochenschr.* **1922**, *44*,1537–1538.
[6] H. Naiki, K. Higuchi, M. Hosokawa, T. Takeda, *Anal. Biochem.* **1989**, *177*, 244–249.
[7] S. D. Styren, R. L. Hamilton, G. C. Styren, W. E. Klunk, *J. Histochem. Cytochem.* **2000**, *48*, 1223–1232.
[8] H. F. Kung, C. W. Lee, Z. P. Zhuang, M. P. Kung, C. Hou, K. Plossl, *J. Am. Chem. Soc.* **2001**, *123*,12740–12741.
[9] W. E. Klunk, H. Engler, A. Nordberg, Y. Wang, G. Blomqvist, D. P. Holt, M. Bergström, I. Savitcheva, G. F. Huang, S. Estrada, B. Ausén, M. L. Debnath, J. Barletta, J. C. Price, J. Sandell, B. J. Lopresti, A. Wall, P. Koivisto, G. Antoni, C. A. Mathis, B. Långström, *Ann. Neurol.* **2004**, *55*, 306–319.
[10] E. E. Nesterov, J. Skoch, B. T. Hyman, W. E. Klunk, B. J. Bacskai, T. M. Swager, *Angew. Chem. Int. Ed.* **2005**, *44*, 5452–5456; *Angew. Chem.* **2005**, *117*, 5588–5592.
[11] K. P. R. Nilsson, *FEBS Lett.* **2009**, *583*, 2593–2599.
[12] A. Åslund, C. J. Sigurdson, T. Klingstedt, S. Grathwohl, T. Bolmont, D. L. Dickstein, E. Glimsdal, S. Prokop, M. Lindgren, P. Konradsson, D. M. Holtzman, P. R. Hof, F. L. Heppner, S. Gandy, M. Jucker, A. Aguzzi, P. Hammarström, K. P. R. Nilsson, *ACS Chem. Biol.* **2009**, *4*, 673–684.
[13] T. Klingstedt, A. Åslund, R. A. Simon, L. B. G. Johansson, J. J. Mason, S. Nyström, P. Hammarström, K. P. R. Nilsson, *Org. Biomol. Chem.* **2011**, *9*, 8356–8370.
[14] T. Klingstedt, H. Shirani, K. O. A. Åslund, N. J. Cairns, C. J. Sigurdson, M. Goedert, K. P. R. Nilsson, *Eur. J. Chem.* **2013**, *19*, 10179–10192.
[15] S. Nyström, K. M. Psonka-Antonczyk, P. G. Ellingsen, L. B. Johansson, N. Reitan, S. Handrick, S. Prokop, F. L. Heppner, B. M. Wegenast-Braun, M. Jucker, M. Lindgren, B. T. Stokke, P. Hammarström, K. P. R. Nilsson, *ACS Chem. Biol.* **2013**, *8*, 1128–1133.
[16] T. Klingstedt, H. Shirani, J. Mahler, B. M. Wegenast-Braun, S. Nyström, M. Goedert, M. Jucker, K. P. R. Nilsson, *Eur. J. Chem.* **2015**, *21*, 9072–9082.
[17] M. Bäck, H. Appelqvist, H. Levine 3rd, K. P. R. Nilsson, *Chemistry* **2016**, *22*, 18335–18338.
[18] J. Rasmussen, J. Mahler, N. Beschorner, S. A. Kaeser, L. M. Häsler, F. Baumann, S. Nyström, E. Portelius, K. Blennow, T. Lashley, N. C. Fox, D. Sepulveda-Falla, M. Glatzel, A. L. Oblak, B. Ghetti, K. P. R. Nilsson, P. Hammarström, M. Staufenbiel, L. C. Walker, M. Jucker, *Proc. Natl. Acad. Sci. USA* **2017**, *114*, 13018–13023.
[19] D. Sehlin, X. T. Fang, S. R. Meier, M. Jansson, S. Syvänen, *Sci. Rep.* **2017**, *7*, 17254.
[20] H. Shirani, H. Appelqvist, M. Bäck, T. Klingstedt, N. J. Cairns, K. P. R. Nilsson, *Chemistry* **2017**, *23*, 17127–17135.
[21] J. D. Ulrich, T. K. Ulland, T. E. Mahan, S. Nyström, K. P. R. Nilsson, V. M. Song, Y. Zhou, M. Reinartz, S. Choi, H. Jiang, F. R. Stewart, E. Anderson, Y. Wang, M. Colonna, D. M. Holtzman, *J. Exp. Med.* **2018**, *215*, 1047–1058.
[22] G. M. de Waal, L. Engelbrecht, T. Davis, W. J. S. de Villiers, D. B. Kell, E. Pretorius, *Sci. Rep.* **2018**, *8*, 16798.
[23] A. B. Wreden, L. Fernandes, M. Kelley, A. Pereira-Neves, C. S. Moreira, D. R. da Rocha, F. L. Palhano, *ACS Chem. Neurosci.* **2018**, *9*, 2807–2814.
[24] W. Michno, S. Nyström, P. Wehrli, T. Lashley, G. Brinkmalm, L. Guerard, S. Syvänen, D. Sehlin, I. Kaya, D. Brinet, K. P. R. Nilsson, P. Hammarström, K. Blennow, H. Zetterberg, J. Hanrieder, *J. Biol. Chem.* **2019**, *294*, 6719–6732.
[25] L. Lantz, H. Shirani, T. Klingstedt, K. P. R. Nilsson, *Chemistry* **2020**, *26*, 7425–7432.
[26] M. Kelley, R. Sant'Anna, L. Fernandes, F. L. Palhano, *ACS Omega* **2021**, 6, 8700–8705.
[27] T. Klingstedt, H. Shirani, B. Ghetti, R. Vidal, K. P. R. Nilsson, *ChemBioChem* **2021**, *22*, 2568–2581.
[28] M. Barth, M. Bacioglu, N. Schwarz, R. Novotny, J. Brandes, M. Welzer, S. Mazzitelli, L. M. Häsler, M. Schweighauser, T. V. Wuttke, D. Kronenberg-Versteeg, K. Fog, M. Ambjørn, A. Alik, R. Melki, P. J. Kahle, D. R. Shimshek, H. Koch, M. Jucker, G. Tanriöver, *Mol. Neurodegener.* **2021**, *16*, 54.
[29] K. Magnusson, R. Simon, D. Sjölander, C. J. Sigurdson, P. Hammarström, K. P. R. Nilsson, *Prion* **2014**, *8*, 319–329.
[30] U. S. Herrmann, A. K. Schütz, H. Shirani, D. Huang, D. Saban, M. Nuvolone, B. Li, B. Ballmer, A. K. Åslund, J. J. Mason, E. Rushing, H. Budka, S. Nyström, P. Hammarström, A. Böckmann, A. Caflisch, B. H. Meier, K. P. R. Nilsson, S. Hornemann, A. Aguzzi, *Sci. Transl. Med.* **2015**, *7*, 299ra123.
[31] A. K. Schütz, S. Hornemann, M. A. Wälti, L. Greuter, C. Tiberi, R. Cadalbert, M. Gantner, R. Riek, P. Hammarström, K. P. R. Nilsson, A. Böckmann, A. Aguzzi, B. H. Meier, *ACS Chem. Neurosci.* **2018**, *9*, 475–481.
[32] C. König, R. Skånberg, I. Hotz, A. Ynnerman, P. Norman, M. Linares, *Chem. Commun.* **2018**, *54*, 3030–3033.
[33] A. K. Schütz, A. Soragni, S. Hornemann, A. Aguzzi, M. Ernst, A. Böckmann, B. H. Meier, *Angew. Chem. Int. Ed. Engl.* **2011**, *50*, 5956–60.
[34] A. W. P. Fitzpatrick, B. Falcon, S. He, A. G. Murzin, G. Murshudov, H. J. Garringer, R. A. Crowther, B. Ghetti, M. Goedert, S. H. W. Scheres, *Nature* **2017**, *547*, 85–190.
[35] B. Falcon, W. Zhang, A. G. Murzin, G. Murshudov, H. J. Garringer, R. Vidal, R. A. Crowther, B. Ghetti, S. H. W. Scheres, M. Goedert, *Nature* **2018**, *561*, 137–140.

[36] B. Falcon, J. Zivanov, W. Zhang, A. G. Murzin, H. J. Garringer, R. Vidal, R. A. Crowther, K. L. Newell, B. Ghetti, M. Goedert, S. H. W. Scheres, *Nature* **2019**, *568*, 420–423.
[37] W. Zhang, A. Tarutani, K. L. Newell, A. G. Murzin, T. Matsubara, B. Falcon, R. Vidal, H. J. Garringer, Y. Shi, T. Ikeuchi, S. Murayama, B. Ghetti, M. Hasegawa, M. Goedert, S. H. W. Scheres, *Nature* **2020**, *580*, 283–287.
[38] Y. Shi, W. Zhang, Y. Yang, A. G. Murzin, B. Falcon, A. Kotecha, M. van Beers, A. Tarutani, F. Kametani, H. J. Garringer, R. Vidal, G. I. Hallinan, T. Lashley, Y. Saito, S. Murayama, M. Yoshida, H. Tanaka, A. Kakita, T. Ikeuchi, A. C. Robinson, D. M. A. Mann, G. G. Kovacs, T. Revesz, B. Ghetti, M. Hasegawa, M. Goedert, S. H. W. Scheres, *Nature* **2021**, *598*, 359–363.
[39] C. Condello, T. Lemmin, J. Stöhr, M. Nick, Y. Wu, A. M. Maxwell, J. C. Watts, C. D. Caro, A. Oehler, C. D. Keene, T. D. Bird, S. G. van Duinen, L. Lannfelt, M. Ingelsson, C. Graff, K. Giles, W. F. DeGrado, S. B. Prusiner, *Proc. Natl. Acad. Sci. USA* **2018**, *115*, E782-E791.
[40] A. A. Stepanchuk, P. A. Barber, T. Lashley, J. T. Joseph, P. K. Stys, *Neurobiol. Dis.* **2021**, *161*, 105540.
[41] H. Liu, C. Kim, T. Haldiman, C. J. Sigurdson, S. Nyström, K. P. R. Nilsson, M. L. Cohen, T. Wisniewski, P. Hammarström, J. G. Safar, *J. Biol. Chem.* **2021**, *297*, 101267.
[42] R. A. Simon, H. Shirani, K. O. A. Åslund, M. Bäck, V. Haroutunian, S. Gandy, K. P. R. Nilsson, *Chemistry* **2014**, *20*, 12537–12543.
[43] H. Shirani, M. Linares, C. J. Sigurdson, M. Lindgren, P. Norman, K. P. R. Nilsson, *Chemistry* **2015**, *21*, 15133–15137.
[44] M. Schmidt, S. Wiese, V. Adak, J. Engler, S. Agarwal, G. Fritz, P. Westermark, M. Zacharias, M. Fändrich, *Nat. Commun.* **2019**, *10*, 5008.
[45] F. Liberta, S. Loerch, M. Rennegarbe, A. Schierhorn, P. Westermark, G. T. Westermark, B. P. C. Hazenberg, N. Grigorieff, M. Fändrich, M. Schmidt, *Nat. Commun.* **2019**, *10*, 1104.
[46] D. Arseni, M. Hasegawa, A. G. Murzin, F. Kametani, M. Arai, M. Yoshida, B. Ryskeldi-Falcon, *Nature* **2021**, *601*, 139.
[47] Y. Todarwal, C. Gustafsson, N. N. Thi Minh, I. Ertzgaard, T. Klingstedt, B. Ghetti, R. Vidal, C. König, M. Lindgren, K. P. R. Nilsson, M. Linares, P. Norman, *J. Phys. Chem. B* **2021**, *125*, 11628–11636.
[48] C. Gustafsson, H. Shirani, P. Leira, D. R. Rehn, M. Linares, K. P. R. Nilsson, P. Norman, M. Lindgren, *ChemPhysChem* **2021**, *22*, 323–335.
[49] F. Prelli, E. Castaño, G. G. Glenner, B. Frangione, *J. Neurochem.* **1988**, *51*, 648–651.
[50] D. M. A. Mann, T. Iwatsubo, Y. Ihara, N. J. Cairns, P. L. Lantos, N. Bogdanovic, L. Lannfelt, B. Winblad, M. L. C. Maat-Schieman, M. N. Rossor, *Am. J. Pathol.* **1996**, *148*, 1257–1266.
[51] E. Gkanatsiou, E. Portelius, C. E. Toomey, K. Blennow, H. Zetterberg, T. Lashley, G. Brinkmalm, *Neurosci. Lett.* **2019**, *701*, 125–131.

Manuscript received: May 19, 2022
Accepted manuscript online: August 11, 2022
Version of record online: September 5, 2022